Inorganic Chemistry
Article

Inorg. Chem. **2010**, *49*, 11317–11324 **11317**
DOI: 10.1021/ic101028n

The Quantum Cutting of Tb^{3+} in $Ca_6Ln_2Na_2(PO_4)_6F_2$ (Ln = Gd, La) under VUV−UV Excitation: with and without Gd^{3+}

Mubiao Xie,[†] Ye Tao,[‡] Yan Huang,[‡] Hongbin Liang,*[,†] and Qiang Su[†]

[†]*MOE Laboratory of Bioinorganic and Synthetic Chemistry, State Key Laboratory of Optoelectronic Materials and Technologies, School of Chemistry and Chemical Engineering, Sun Yat-sen University, Guangzhou 510275, P. R. China, and* [‡]*Beijing Synchrotron Radiation Facilities, Institute of High Energy Physics, Chinese Academy of Science, Beijing 100039, P. R. China*

Received May 20, 2010

The VUV−vis spectroscopic properties of Tb^{3+} activated fluoro-apatite phosphors $Ca_6Ln_{2-x}Tb_xNa_2(PO_4)_6F_2$ (Ln = Gd, La) were studied. The results show that phosphors $Ca_6Gd_{2-x}Tb_xNa_2(PO_4)_6F_2$ with Gd^{3+} ions as sensitizers have intense absorption in the VUV range. The emission color of both phosphors can be tuned from blue to green by changing the doping concentration of Tb^{3+} under 172 nm excitation. The visible quantum cutting (QC) via cross relaxation between Tb^{3+} ions was observed in cases with and without Gd^{3+}. Though QC can be realized in phosphors $Ca_6La_{2-x}Tb_xNa_2(PO_4)_6F_2$, we found that Gd^{3+}-containg phosphors have a higher QC efficiency, confirming that the Gd^{3+} ion indeed plays an important role during the quantum cutting process. In addition, the energy transfer process from Gd^{3+} to Tb^{3+} as well as $^5D_3$—$^5D_4$ cross relaxation was investigated and discussed in terms of luminescence spectra and decay curves.

1. Introduction

The plasma resonance vacuum ultraviolet (VUV) radiation lines of Xe atoms at 147 nm and Xe_2 molecules at 172 nm are required to excite phosphors with blue, green, and red tricolor emissions for application in plasma display panels (PDPs) and Hg-free lamps.[1] The most available commercial phosphors for PDPs are (Y,Gd)BO_3:Eu^{3+} (YGB) for red, Zn_2SiO_4:Mn^{2+} (ZSM) for green, and $BaMgAl_{10}O_{17}$:Eu^{2+} (BAM) for blue.[2−4] The common shortcoming of them is low emission efficiency. So it is urgent to search for highly efficient tricolor phosphors for PDPs and Hg-free lamps. In a proper host, Tb^{3+} is expected to exhibit intense green emission under VUV excitation; therefore it might be used as a green emission component in these devices. Moreover, Tb^{3+} emission can be tuned along a large color gamut from blue to green by the well-known cross relaxation energy transfer process, which is dependent on the doping concentration of Tb^{3+} and host lattices.[5−8]

When a highly energetic VUV photon is used to excite a phosphor in PDPs or Hg-free lamps, it inherently limits the energy efficiency of phosphor if only one visible photon is generated after an absorbed-VUV photon. Therefore, new phosphors with quantum efficiencies greater than 100% are required for this purpose. A quantum-cutting (QC) phosphor would therefore serve this need. As for Tb^{3+} ions, the quantum cutting process has been confirmed in some fluorides and phosphates like K_2GdF_5:Tb^{3+},[9] $BaGdF_5$:Tb^{3+},[10] $GdPO_4$:Tb^{3+}, $Sr_3Gd(PO_4)_3$:Tb^{3+},[11] and Li(Y, Gd)$(PO_3)_4$.[12] These Tb^{3+}-QC phosphors share a feature. That is, they contain Gd^{3+} ions.

In our previous work,[13] an intensive green-emission phosphor, $Ca_6Gd_{1.5}Tb_{0.50}Na_2(PO_4)_6F_2$, had been reported for PDP application. In this paper, two series of phosphors, $Ca_6Ln_{2-x}Tb_xNa_2(PO_4)_6F_2$ (Ln = Gd, La), one with Gd^{3+} and another without Gd^{3+}, are synthesized. According to the

*To whom correspondence should be addressed. E-mail: cesbin@mail.sysu.edu.cn.

(1) Höppe, H. A. *Angew. Chem., Int. Ed.* **2009**, *48*, 3572–3582.
(2) Kim, C. H.; Kwon, I. E. C.; Park, H.; Hwang, Y. J.; Bae, H. S.; Yu, B. Y.; Pyun, C. H.; Hong, G. Y. *J. Alloys Compd.* **2000**, *311*, 33–39.
(3) Jüstel, T.; Krupa, J. C.; Wiechert, D. U. *J. Lumin.* **2001**, *93*, 179–189.
(4) Zhang, S. X. *IEEE Trans. Plasma Sci.* **2006**, *34*, 294–304.
(5) Tian, Z. F.; B.iang, L H.; Chen, W. P.; Su, Q.; Zhang, G. B.; Yang, G. T. *Opt. Express.* **2009**, *17*, 956–962.
(6) Hao, Z. D.; Zhang, J. H.; Zhang, X.; Lu, S. Z.; Wang, X. J. *J. Electrochem. Soc.* **2009**, *156*, 193–196.
(7) Liu, X. M.; Pang, R.; Quan, Z. W.; Yang, J.; Lin, J. *J. Electrochem. Soc.* **2007**, *154*(7), J185–J189.
(8) Liu, X. M.; Lin, J. *J. Mater.Chem.* **2008**, *18*, 221–228.
(9) Lee, T. J.; Luo, L. Y.; Diau, E. W. G.; Chen, T. M.; Cheng, B. M.; Tung, C. Y. *Appl. Phys. Lett.* **2006**, *89*, 131121.
(10) Tzeng, H. Y.; Cheng, B. M.; Chen, T. M. *J. Lumin.* **2007**, *122−123*, 917–920.
(11) Wang, D. Y.; Kodama, N. *J. Solid State Chem.* **2009**, *182*, 2219–2224.
(12) Han, B.; Liang, H. B.; Huang, Y.; Tao, Y.; Su, Q. *J. Phys. Chem. C.* **2010**, *114*, 6770–6777.
(13) Xie, M. B.; Liang, H. B.; Han, B.; Chen, W. P.; Su, Q.; Huang, Y.; Gao, Z. H.; Tao, Y. *Opt. Lett.* **2009**, *34*, 3466–3468.

Published on Web 11/11/2010

viewpoint on Tb^{3+}-QC in references, the quantum cutting of Tb^{3+} seems not to deal with Gd^{3+} ions. But in references, these Tb^{3+}-QC phosphors usually have Gd^{3+} ions.[9−12] So we will focus on the effect of Gd^{3+} in quantum cutting by comparing the spectra of samples with and without Gd^{3+}. In addition, as a continuous work,[13] we will discuss the tunable emission of the phosphors at different doping levels and the $Gd^{3+}\rightarrow Tb^{3+}$ energy transfer.

2. Experimental Section

2.1. Synthesis. A series of samples, $Ca_6Ln_{2-x}Tb_xNa_2(PO_4)_6F_2$ (Ln = Gd, La, x = 0.001, 0.005, 0.01, 0.05, 0.10, and 0.50), was prepared using a solid-state reaction technique at high temperatures. The starting materials are analytical-grade $CaCO_3$, $NH_4H_2PO_4$, NH_4F, Na_2CO_3, and rare earth oxides (La_2O_3, Gd_2O_3, Tb_4O_7, 99.99% purity). The stoichiometric raw materials were ground thoroughly in an agate mortar and were fired at 1050 °C in a CO atmosphere for 4 h. White powder samples were obtained when the products cooled down to room temperature (RT) by switching off the muffle furnace and were ground in an agate mortar again.

2.2. Characterizations. The phase purity and structure of the samples were characterized by a powder X-ray diffraction (XRD) analysis with Cu Kα (λ = 1.5405 Å) radiation on a Rigaku D/max 2200 vpc X-ray Diffractometer. Fourier transform infrared (FT-IR) spectra were measured on a Nicolet Avatrar 330 spectrophotometer with the KBr pellet technique in the wavenumber range of 4000−400 cm^{-1}.

The UV-excited luminescence spectra and luminescence decay curves at RT were recorded on an Edinburgh FLS 920 combined fluorescence lifetime and steady state spectrometer, which was equipped with a time-correlated single-photon counting (TCSPC) card. A 450 W xenon lamp was used as the excitation source. For the measurements of luminescence decays, the excitation photons were provided by a 60 W μF900 microsecond flash lamp with a pulse width of 1.5−3.0 μs and a pulse repetition rate of 50 Hz.

The VUV spectra were recorded online at Beamline 4B8 at the Beijing Synchrotron Radiation Facilities (BSRF) by remote access under the dedicated synchrotron mode (2.5 GeV, 100−400 mA). The synchrotron radiation excitation light was dispersed through a 1 m Seya monochromator (1200 grooves/mm, 120−350 nm, 1 nm bandwidth). The emission light was spectrally filtered using an Acton Model SP-308 monochromator (600 grooves/mm, 330−900 nm). The signal was detected with a Hamamatsu Model H8259−01 photon counting unit. The vacuum in the sample chamber was about 1×10^{-5} mbar. Thirteen samples can be simultaneously put in a sample chamber, and the excitation light from the monochromator was divided into two beams: one is to excite our sample and another is to excite the standard sample sodium salicylate (4S, o-$C_6H_4OHCOONa$). By this arrangement, our sample and 4S can be excited at the same time. Moreover, a program at the station simultaneously corrected the effect of the experimental setup response on the relative VUV excitation intensities by dividing the measured excitation intensities of our sample with that of 4S under the same excitation conditions. For all excitation and emission spectra discussed below, we have normalized all parameters, which include (emission and excitation) slit width, integrating time, beam intensity, and the relative intensity of energy at the excitation wavelength.

3. Results

3.1. XRD Patterns and FT-IR Spectra Analysis. $Ca_6Ln_2Na_2(PO_4)_6F_2$ is an apatite-type compound.[14−16] Apatites contain a large number of inorganic compounds with the general formula $M_{10}(XO_4)_6Y_2$ (M = alkaline earth, Pb, alkali, rare earth, etc.; X = P, As, Si, Ge, S, V, Mn, etc.; and Y = OH, halogen, (1/2)O, (1/2)S, (1/2)CO_3, etc.).[17,18] The XRD measurements were carried out to check the phase purity. The XRD patterns of the representative samples $Ca_6Gd_{2-x}Tb_xNa_2(PO_4)_6F_2$ (a, x = 0.001; b, x = 0.50) and $Ca_6La_{2-x}Tb_xNa_2(PO_4)_6F_2$ (c, x = 0.001; d, x = 0.50) were plotted in Figure 1, showing that all samples are of single phase and match well with the JCPDS card (No. 71-0881) [$Ca_5(PO_4)_3F$]. This indicates that doping Tb^{3+} ions have no obvious effect on the crystal structure.

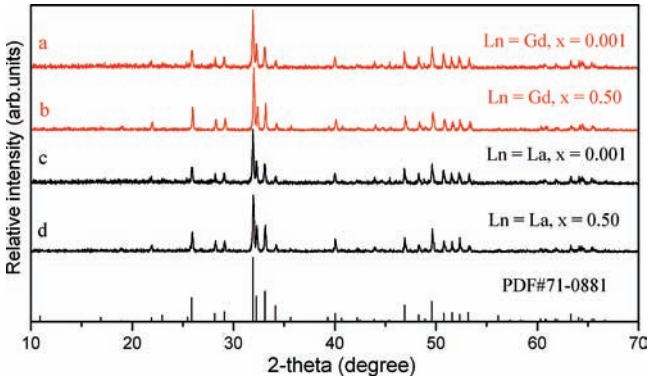

Figure 1. XRD patterns of samples $Ca_6Gd_{2-x}Tb_xNa_2(PO_4)_6F_2$ (a, x = 0.001; b, x = 0.50) and $Ca_6La_{2-x}Tb_xNa_2(PO_4)_6F_2$ (c, x = 0.001; d, x = 0.50).

To get the frequency of effective phonons for multiphonon relaxation, the Fourier transform infrared (FT-IR) spectra of compounds $Ca_6Ln_2Na_2(PO_4)_6F_2$ and $Ca_6Ln_{1.95}Tb_{0.50}Na_2(PO_4)_6F_2$ (Ln = Gd, La) were measured and are shown in Figure 2. These spectra share a similar shape. The band at 440 cm^{-1} is assigned to the ν_2 phosphate mode; those at 565 and 606 cm^{-1} are derived from the ν_4 bending vibration of the P−O mode. The strong bands at 1048 cm^{-1} are due to the triply degenerate ν_3 antisymmetric P−O stretching vibration of the PO_4^{3-} groups, which we consider the frequency of effective phonons in a later discussion. The bands centered at about 3430 cm^{-1} may be due to the water adsorbed on the surface of the samples.

3.2. Photoluminescence Properties and Tunable Emission. The VUV−vis excitation spectra (λ_{em} = 379 nm) of $Ca_6Gd_{1.995}Tb_{0.005}Na_2(PO_4)_6F_2$ and $Ca_6La_{1.995}Tb_{0.005}Na_2(PO_4)_6F_2$ are given in curves a−c of Figure 3I. Two broad bands can be observed in curve a for phosphor $Ca_6Gd_{1.995}Tb_{0.005}Na_2(PO_4)_6F_2$: the short-wavelength one begins at ~192 nm with a maximum at ~172 nm; the long-wavelength one starts at ~243 nm with a maximum at ~220 nm. We assign the former the host-related absorption and the latter the spin-allowed f−d ($^7F\rightarrow{}^7D$) transitions of Tb^{3+} in the host lattice according to our previous work.[13,17,19] The sharp lines at about 195, 202, 246, 253, 273, and 312 nm are from the f−f transitions of Gd^{3+}. In curve a, a rather broad weak band from ~250 nm to ~320 nm is detected, we consider it as being from unknown impurities

(14) Mayer, I.; Roth, R. S.; Brown, W. E. *J. Solid State Chem.* **1974**, *11*, 33–37.
(15) Mayer, I.; Cohen, S. *J. Solid State Chem.* **1983**, *48*, 17–20.
(16) Toumi, M.; Dogguy, L. S.; Bulou, A. *J. Solid State Chem.* **2000**, *149*, 308–313.
(17) Liang, H. B.; Zeng, Q.; Tian, Z. F.; Lin, H. H.; Su, Q.; Zhang, G. B.; Fu, Y. B. *J. Electrochem. Soc.* **2007**, *154*, J177.
(18) Zhang, J. H.; Liang, H. B.; Su, Q. *J. Phys. D: Appl. Phys.* **2009**, *42*, 105110.
(19) Zhong, J. P.; Liang, H. B.; Han, B.; Su, Q.; Tao, Y. *Chem. Phys. Lett.* **2008**, *453*, 192.

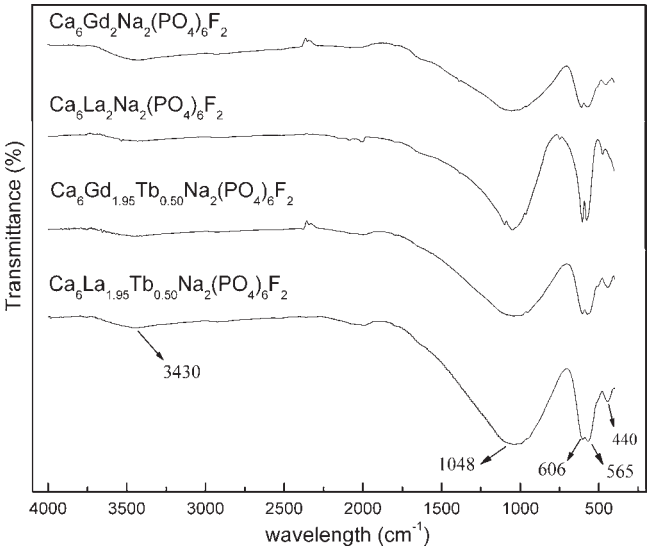

Figure 2. FT-IR spectra of compounds $Ca_6Ln_2Na_2(PO_4)_6F_2$ and $Ca_6Ln_{1.95}Tb_{0.50}Na_2(PO_4)_6F_2$ (Ln = Gd, La).

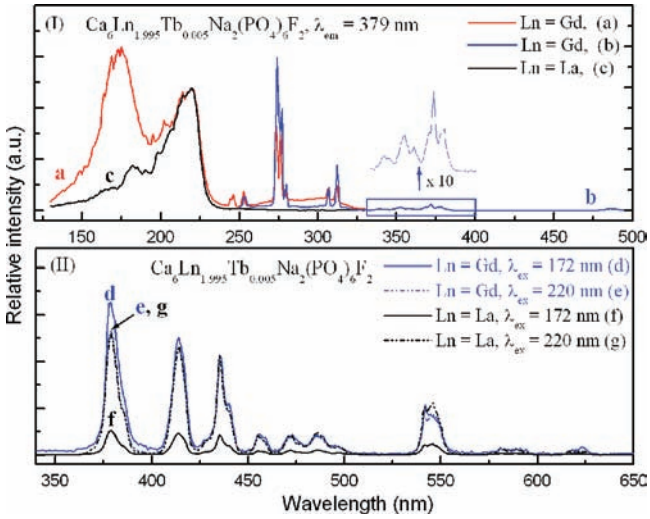

Figure 3. The VUV−vis excitation spectra (a−c, λ_{em} = 379 nm) and emission spectra under VUV−UV excitation (d, f: λ_{ex} = 172 nm; e, g: λ_{ex} = 220 nm) for samples $Ca_6Ln_{1.995}Tb_{0.005}Na_2(PO_4)_6F_2$ (Ln = Gd, La).

which are introduced to the sample when we measured this spectrum, because this band was not observed in curve b. In addition, the f−f excitation transitions of Tb^{3+} in the range from 330 to 400 nm are found in the magnified spectrum of curve b.

Comparing curve a with curve c, we can find that the intensities of the f−d transitions of Tb^{3+} (~220 nm) in two phosphors $Ca_6Gd_{1.995}Tb_{0.005}Na_2(PO_4)_6F_2$ and $Ca_6La_{1.995}Tb_{0.005}Na_2(PO_4)_6F_2$ are almost the same, but the host-related absorptions are quite different. Although the host-related absorptions are onset at the same wavelength (~192 nm) for two phosphors, their intensities are evidently different. A weaker absorption band can be seen in phosphor $Ca_6La_{1.995}Tb_{0.005}Na_2(PO_4)_6F_2$. The same onset of the host-related absorption implies that the band gap is the same for Gd-containing compound $Ca_6Gd_2Na_2(PO_4)_6F_2$ and La-containing compound $Ca_6La_2Na_2(PO_4)_6F_2$. The stronger host-related absorption of $Ca_6Gd_{1.995}Tb_{0.005}Na_2(PO_4)_6F_2$ relative to that of $Ca_6La_{1.995}Tb_{0.005}Na_2(PO_4)_6F_2$ seems to suggest that the energy transfer efficiency from host to luminescent centers is higher for Gd-containing phosphor than that for La-containing phosphor. We think two main factors, the higher excited 4f multiplets of Gd^{3+} in this range and the intermediate role of Gd^{3+} in the energy transfer process, are responsible for the stronger host-related absorption of $Ca_6Gd_{1.995}Tb_{0.005}Na_2(PO_4)_6F_2$, as will be discussed later.[20−22]

Under 172 and 220 nm excitation, both $Ca_6Gd_{1.995}Tb_{0.005}Na_2(PO_4)_6F_2$ and $Ca_6La_{1.995}Tb_{0.005}Na_2(PO_4)_6F_2$ mainly show $^5D_3$ to $^7F_{6,5,4,3,2}$ transitions with the same patterns as displayed in curves d−g of Figure 3II. Under 172 nm excitation, the luminescence intensity of $Ca_6Gd_{1.995}Tb_{0.005}Na_2(PO_4)_6F_2$ is distinctly stronger than that of $Ca_6La_{1.995}Tb_{0.005}Na_2(PO_4)_6F_2$. Upon 220 nm excitation, curve e and curve f share nearly the same intensity. The relative intensities of both samples at different excitations are consistent with the absorption intensities of 172 and 220 nm in curves a and c.

It is known that the Tb^{3+} ion can be used as an activator in blue phosphors when the emission is mainly from the $^5D_3$ excited level and as green phosphors when the emission is mainly from the $^5D_4$ excited level. The main factors influencing the relative intensity between $^5D_3$ and $^5D_4$ emission are the Tb^{3+} concentration, the distance between the adjacent Tb^{3+} ions, the temperature, and the vibration energy of the host lattice. At low concentrations, it mainly emits blue light from the $^5D_3$ excited level, but at higher concentrations, the $^5D_3$ emission will be quenched by cross relaxation ($^5D_3 + {}^7F_6 \rightarrow {}^5D_4 + {}^7F_0$) and multiphonon relaxation, resulting in strong green emission from the $^5D_4$ excited level.[9] Figure 4 shows the emission spectra of samples $Ca_6Ln_{2-x}Tb_xNa_2(PO_4)_6F_2$ with different Tb^{3+} concentrations (x value) under 172 nm excitation. For both samples, the Tb^{3+} $^5D_3 \rightarrow {}^7F_J$ and $^5D_4 \rightarrow {}^7F_J$ transitions can be observed, respectively. However, the emission intensity ratio of $^5D_4$ to $^5D_3$ increases with the increasing of Tb^{3+} content, mainly due to the cross relaxation process between neighboring Tb^{3+} ions [the multiphonon relaxation may be also a channel, because the frequency of effective phonons is ~1048 cm^{-1} for $Ca_6Ln_2Na_2(PO_4)_6F_2$, as shown in FT-IR spectra in Figure 2]. The dependence of emission intensities of $^5D_3$ and $^5D_4$ levels on the Tb^{3+} doping content upon 172 nm excitation is shown in Figure 5. For both phosphors, the emission intensity of $^5D_3$ is stronger than that of $^5D_4$ at a relatively low Tb^{3+} doping content (below 1.0 mol %). At about a 5 mol % Tb^{3+} content, the intensity of $^5D_3$ emission is nearly the same as that of $^5D_4$ emission. Then, the $^5D_4$ emission increases fast, and $^5D_3$ emission decreases rapidly. Therefore, the color of both samples, $Ca_6Gd_{2-x}Tb_xNa_2(PO_4)_6F_2$ and $Ca_6La_{2-x}Tb_xNa_2(PO_4)_6F_2$, can be tuned from blue (with chromaticity coordinates $x \approx 0.21$, $y \approx 0.19$) to yellowish-green (0.30, 0.59) by changing the doping concentration of Tb^{3+} ions. The luminescence photographs in the top insets of Figure 5 present their images in terms of Tb^{3+} doping contents.

(20) Peijzel, P. S.; Vermeulen, P.; Schrama, W. J. M.; Meijerink, A.; Reid, M. F.; Burdick, G. W. *Phys. Rev. B* **2005**, *71*, 125126.
(21) Maylot, A.; Zhang, W.; martin, P.; Chassigneux, B.; Krupa, J. C. *J. Electrochem. Soc.* **1996**, *143*(1), 330–333.
(22) Hair, J. Th. W. de; Konijnendijk, W. L. *J. Electrochem. Soc.* **1980**, *127*(1), 161–164.

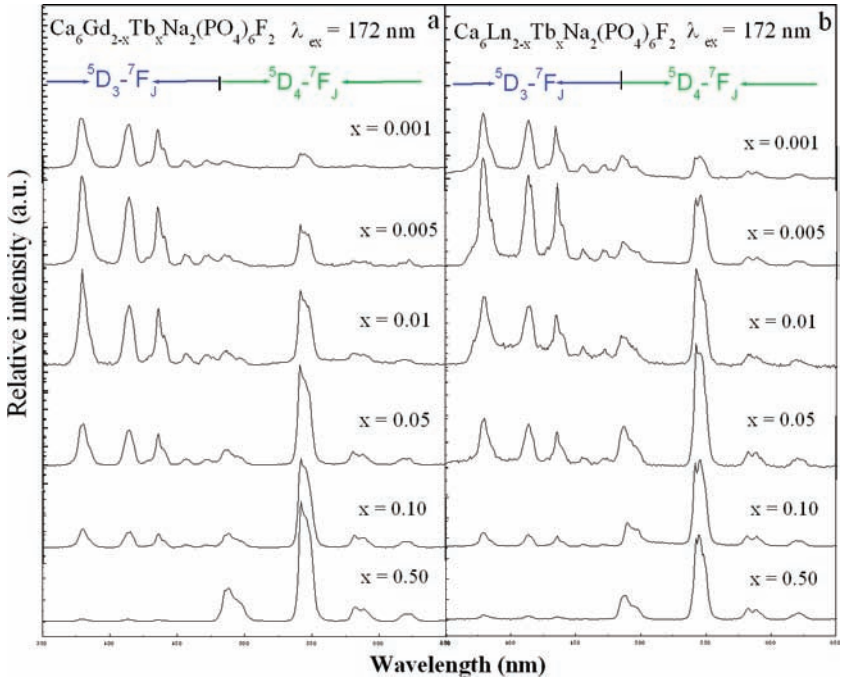

Figure 4. Emission spectra of $Ca_6Ln_{2-x}Tb_xNa_2(PO_4)_6F_2$ (a, Ln = Gd; b, Ln = La) with different x values under 172 nm excitation.

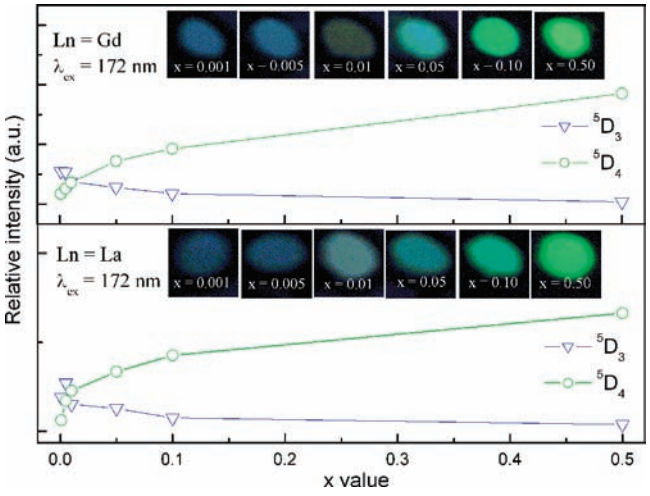

Figure 5. Emission intensities of Tb^{3+} $^5D_3$ and $^5D_4$ levels as a function of x values in $Ca_6Ln_{2-x}Tb_xNa_2(PO_4)_6F_2$ (Ln = Gd, La) phosphors with 172 nm excitation. Top insets present the photography images.

3.3. Energy Transfer from Gd^{3+} to Tb^{3+}. The Gd^{3+} ion was studied as an efficient energy transfer (ET) ion in Tb^{3+} activated phosphors.[23,24] To analyze the ET of $Gd^{3+}\rightarrow Tb^{3+}$, the luminescence decay curves of Gd^{3+} $^6P\rightarrow{}^8S_{7/2}$ transitions under 273 nm excitation as a function of x values in $Ca_6Gd_{2-x}Tb_xNa_2(PO_4)_6F_2$ were measured as shown in Figure 6a. A near single-exponential decay process was observed with different Tb^{3+} contents. Additionally, a small deviation from exponential decay also occurs in pure $Ca_6Gd_2Na_2(PO_4)_6F_2$. For curve 1, the deviation may result from such factors as multisites of Gd^{3+} in the host lattice, the slow $Gd^{3+}-Gd^{3+}$ energy diffusion, and unknown defects/impurities.[25,26] From curve 1 to curve 7, the Gd^{3+} decay became faster as the Tb^{3+} ion concentration increased; the corresponding fluorescence lifetimes are calculated and shown in Figure 6b. This phenomenon indicates that much more efficient energy transfer from Gd^{3+} to Tb^{3+} ions occurs in high Tb^{3+} content samples.

The Gd^{3+}-to-Tb^{3+} energy transfer probability ($K_{Gd\rightarrow Tb}$) can be estimated according to the eq 1:[24,27]

$$K_{Gd\rightarrow Tb} = \left(\frac{1}{\tau}\right) - \left(\frac{1}{\tau_0}\right) \quad (1)$$

where τ and τ_0 are the Gd^{3+} donor lifetime in the presence of a Tb^{3+} acceptor and the intrinsic fluorescence lifetime of Gd^{3+} ($x = 0$), respectively. Furthermore, the energy transfer efficiency ($\eta_{Gd\rightarrow Tb}$) is evaluated as[6,28]

$$\eta_{Gd\rightarrow Tb} = 1 - \left(\frac{\tau}{\tau_0}\right) \quad (2)$$

The $K_{Gd\rightarrow Tb}$ and $\eta_{Gd\rightarrow Tb}$ values were calculated according to eqs 1 and 2 and are illustrated in curves a and b in Figure 7, respectively. It can be found that the energy transfer rate and efficiencies of $Gd^{3+}\rightarrow Tb^{3+}$ increase with the increase in Tb^{3+} concentration, indicating that the energy transfer process from Gd^{3+} to Tb^{3+} becomes more and more efficient as the Tb^{3+} concentration increases.

The luminescence decay curves of the Tb^{3+} $^5D_3\rightarrow{}^7F_6$ transition (378 nm) for different Tb^{3+} concentrations are

(23) Chen, L.; Jiang, Y.; Chen, S. F.; Zhang, G. B.; Wang, C.; Li, G. H. *J. Lumin.* **2008**, *128*, 2048–2052.
(24) Li, Y. C.; Chang, Y. H.; Chang, Y. S.; Lin, Y. J.; Laing, C. H. *J. Phys. Chem. C* **2007**, *111*, 10682–10688.
(25) Meijerink, A.; Sytsma, J.; Blasse, G.; Meyer, G.; Stenzel, F. *J. Phys. Chem. Solids* **1992**, *53*, 1147–1152.
(26) van Schaik, W.; van Heek, M. M. E.; Middel, W.; Blasse, G. *J. Lumin.* **1995**, *63*, 103–115.
(27) Ananias, D.; Kostova, M.; Paz, F. A. A.; Ferreira, A.; Carlos, L. D.; Klinowski, J.; Rocha, J. *J. Am. Chem. Soc.* **2004**, *126*, 10410–10417.
(28) Reisfeld, R.; Greenberg, E.; Velapoldi, R.; Barnett, B. *J. Chem. Phys.* **1973**, *56*, 1698–1750.

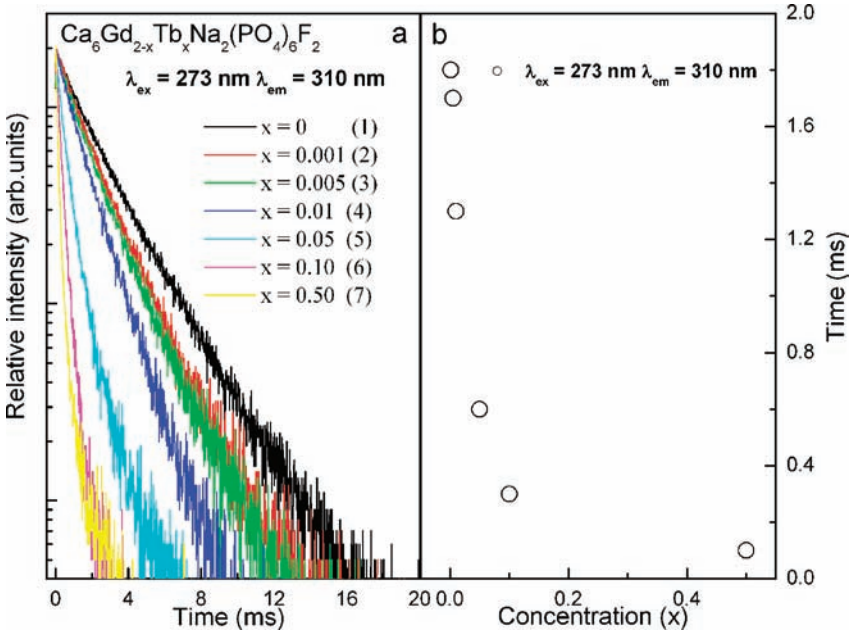

Figure 6. Decay curves (a) and fluorescence lifetimes (b) of Gd^{3+} $^6P-^8S_{7/2}$ transitions under 273 nm excitation as a function of x values in $Ca_6Gd_{2-x}Tb_xNa_2(PO_4)_6F_2$.

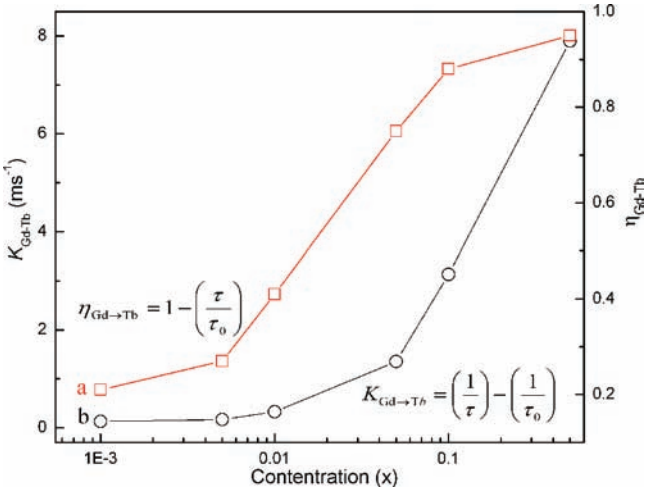

Figure 7. Dependence of the energy transfer probability ($K_{Gd\to Tb}$) (a) and efficiency ($\eta_{Gd\to Tb}$) (b) in $Ca_6Gd_{2-x}Tb_xNa_2(PO_4)_6F_2$ with different x values.

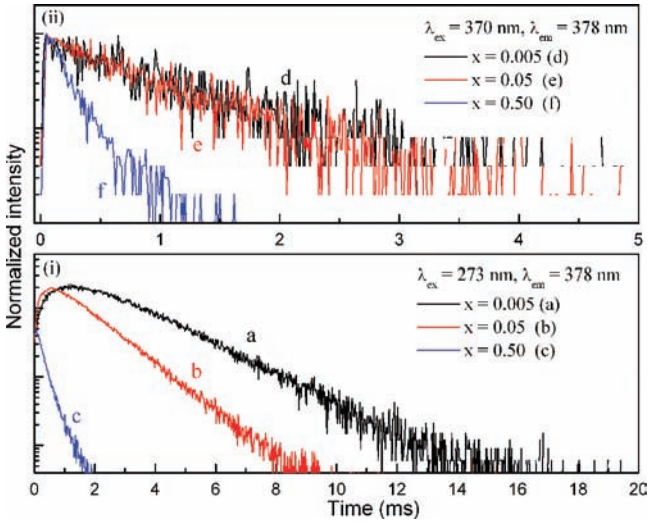

Figure 8. Normalized decay curves of $^5D_3\to^7F_6$ transition under 273 and 370 nm excitation in $Ca_6Gd_{2-x}Tb_xNa_2(PO_4)_6F_2$ as a function of x values.

shown in Figure 8. In these decay measurements, luminescence was excited to two different energy levels of Gd^{3+} ^6I_J (273 nm) and Tb^{3+} $^5L_{10}$ (370 nm).

As seen in curve a of Figure 8i, upon Gd^{3+} ^6I_J excitation, the intensity of the Tb^{3+} $^5D_3\to^7F_6$ emission slowly rises within the initial ~2 ms and then decays exponentially. The initial rising process corresponds to the population of the Tb^{3+} $^5D_3$ level through Gd^{3+}. This phenomenon reinforces the existence of effective energy transfer from Gd^{3+} to Tb^{3+}. As the Tb^{3+} concentration increases to $x = 0.05$, the initial populating time is shortened and the decay of the $^5D_3\to^7F_6$ transition becomes faster (curve b). When the Tb^{3+} content further increases to $x = 0.5$, the population process was undetectable, and just a more rapid decay was observed (curve c). The decay curves under 370 nm excitation (Figure 8ii) are quite different from that under 273 nm excitation. The initial rising process was not found in curves d−f. Nearly single exponential decays (curves d, e) were observed at low Tb^{3+} concentrations, but the deviation from exponential decay was more evident for the high-doping sample (curve f), which indicates that more than one relaxation process exists and its influence on the decay is more clear for the concentrated sample. When the Tb^{3+} concentration is low, the Tb^{3+} $^5D_3\to^7F_6$ transition is dominant; the nearly single exponential decay curves mainly exhibit the luminescence feature of the Tb^{3+} $^5D_3\to^7F_6$ transition. With an increase in the Tb^{3+} concentration, the distance between Tb^{3+} ions decreases, resulting in the $^5D_3-^5D_4$ cross-relaxation energy transfer (CRET) between Tb^{3+} ions becoming more frequent. Thus, the decay rate becomes faster and exhibits a nonexponential decay.[10,19]

Figure 9 shows the decay curves of the $^5D_4\to^7F_5$ transition of Tb^{3+} under excitation at the Gd^{3+} ^6I_J (273 nm),

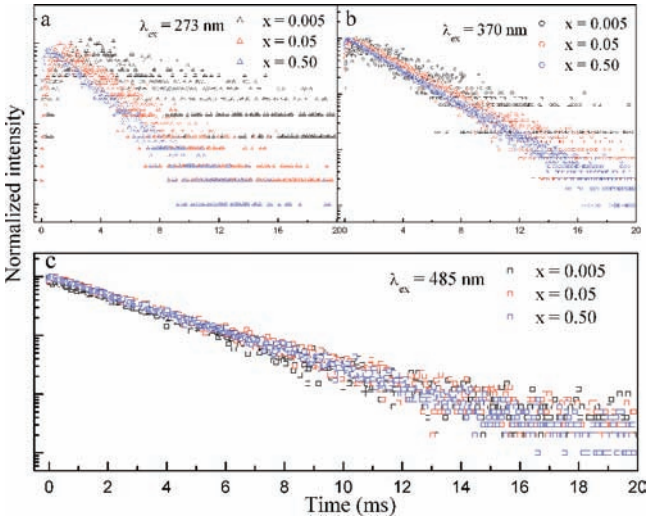

Figure 9. Normalized decay curves of the $^5D_4 \rightarrow {}^7F_5$ transition under 273, 370, and 485 nm excitation in $Ca_6Gd_{2-x}Tb_xNa_2(PO_4)_6F_2$ as a function of x values.

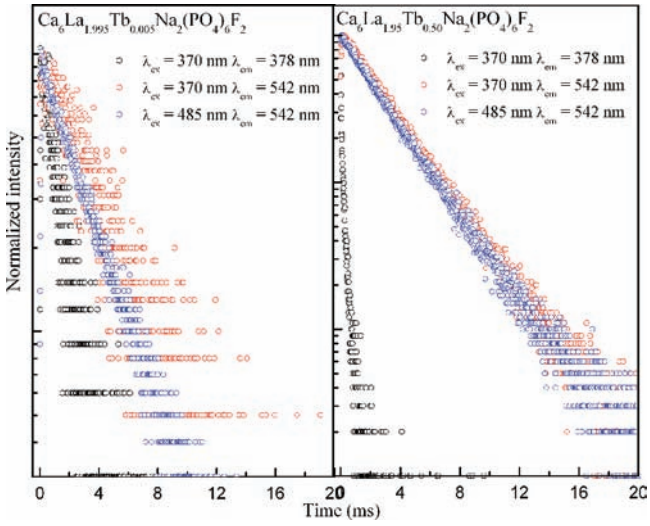

Figure 10. Normalized decay curves of $^5D_3$ and $^5D_4$ levels under 370 and 485 nm excitation in $Ca_6La_{2-x}Tb_xNa_2(PO_4)_6F_2$ as a function of x values.

Tb^{3+} $^5L_{10}$ (370 nm), and Tb^{3+} $^5D_4$ (486 nm) levels. Upon excitation at the Gd^{3+} ^6I_J (273 nm, in Figure 9a) level, the intensity of the $^5D_4 \rightarrow {}^7F_5$ transition shows a rising process initially at a low doping level ($x = 0.005$), and the process gets much more rapid as the Tb^{3+} concentration increases. This rising must be originating from the energy transfer from Gd^{3+} to Tb^{3+} ions, which is similar to the cases of the Tb^{3+} $^5D_3 \rightarrow {}^7F_6$ transition under 273 nm excitation (Figure 8a−c) as discussed above. Under excitation at the Tb^{3+} $^5L_{10}$ (370 nm, Figure 9b) level, the initial rise phenomenon was also detected, and this initial rise became shorter as the Tb^{3+} concentrations got higher, which was due to the much faster cross-relaxation rate between $^5D_3$ and $^5D_4$. In addition, the decay performances under 486 nm excitation, which directly excites the Tb^{3+} $^5D_4$ levels, were measured. As seen in Figure 9c, a single-exponential decay process was observed with different x values, and the decay time was kept constant at about 2.8 ms.

The decays of $Ca_6La_{2-x}Tb_xNa_2(PO_4)_6F_2$ under 370 and 485 nm excitation were also measured, as seen in Figure 10. It is found that the decay curves of $Ca_6La_{2-x}Tb_xNa_2(PO_4)_6F_2$ have a similar performance to that of $Ca_6Gd_{2-x}Tb_xNa_2(PO_4)_6F_2$.

4. Discussion

Quantum cutting (QC) provides an approach to obtain more than one photon for each photon absorbed.[29] The quantum efficiency can be increased using the quantum cutting process via cross-relaxation energy transfer. The quantum cutting of Tb^{3+}-containing phosphors has been demonstrated in some fluorides and phosphates like K_2GdF_5:Tb^{3+},[9] $BaGdF_5$:Tb^{3+},[10] $GdPO_4$:Tb^{3+}, $Sr_3Gd(PO_4)_3$:Tb^{3+},[11] and Li(Y,Gd)$(PO_3)_4$.[12] These phosphors share a compositional feature. That is, they all have Gd^{3+} ions in the hosts. In these systems, proofs of the QC were provided by comparing the Tb^{3+} emission intensity ratios of $^5D_4$ to $^5D_3$ by exciting the 5d energy level of Tb^{3+} or host absorption and the ^6I_J level of Gd^{3+} at 273 nm. In the literature, the schematic energy levels of Gd^{3+} and Tb^{3+} shown in Figure 11 were used to illustrate the QC and energy transfer (ET) processes. When an electron is excited to ^6I_J and/or ^6P_J of Gd^{3+} (process 1), the ^5D states of Tb^{3+} can be populated by direct ET from Gd^{3+} (process 3) and then yield $^5D_3/^5D_4$ emissions (process 4) after the multiphoton relaxation and cross relaxation (process 5). At this moment, the emission intensity ratio of $^5D_4$ to $^5D_3$ remains invariable at a specific doping concentration. However, after a Tb^{3+} ion is directly excited to its 5d state, if the lowest $^7D_J \rightarrow {}^5D_3$ transition and $^7F_6 \rightarrow {}^5D_4$ transition share a near equal energy gap, another type of cross relaxation, Tb^{3+} (^7D_J) + Tb^{3+} ($^7F_6$)$\rightarrow Tb^{3+}$ ($^5D_3$) + Tb^{3+} ($^5D_4$) (process 7), may occur. Therefore, the $^5D_4$ state is populated through this cross relaxation process. Under Tb^{3+} 5d states or host absorption excitation, the $^5D_4$ emission results from processes 4 and 8, while when excited to the Gd^{3+} ^6I or the $^5D_2$, $^5G_4$, or $^5L_9$ states of Tb^{3+}, emission just comes from process 4. Hence, the intensity of $^5D_4$ emission will be enhanced upon 220 and 172 nm excitation relative to that upon 273 or 352 nm excitation for a sample with a specific doping concentration. More than one emitting photon will be generated, and the quantum efficiency of Tb^{3+} can exceed 100% upon excitation to its 5d state in theory.

In spite of the Gd^{3+}-containing characteristics for all Tb^{3+}-QC cases in references,[9−12] Gd^{3+} ions seem to play no role in the quantum cutting process when we accept the above viewpoint. Because the QC is thought to be fulfilled by a Tb^{3+} (^7D_J) + Tb^{3+} ($^7F_6$)$\rightarrow Tb^{3+}$ ($^5D_3$) + Tb^{3+} ($^5D_4$) resonance-type ET process, the emission intensity under the Gd^{3+} ^6I state excitation is just a reference to evaluate the QC. This gives rise to a puzzle: whether the Gd^{3+} ions are really indispensable in the QC process of these Tb^{3+}-containing phosphors. In other words, can the QC be realized for a phosphor without Gd^{3+}? To give an answer for this question, we perform the following measurements.

Figure 12 exhibits the emission spectra of phosphors $Ca_6Gd_{2-x}Tb_xNa_2(PO_4)_6F_2$ ($x = 0.10, 0.50$) under 172, 220, 273, and 352 (near the $^5D_2$, $^5G_4$, $^5L_9$ states of Tb^{3+}) nm excitation and that of phosphors $Ca_6La_{2-x}Tb_xNa_2(PO_4)_6F_2$ ($x = 0.50, 0.90$) under 172, 220, and 352 nm excitation. To compare the emission intensity ratio of $^5D_4$ to $^5D_3$, the spectra were normalized to the height of Tb^{3+} $^5D_3 \rightarrow {}^7F_6$ emissions at

(29) Meltzer, R. S. *Phosphor Handbook*, 2nd ed.; Auspices of Phosphor Research Society: Washington, DC,1998.

379 nm. We find that the emission from the $^5D_4$ level under 172 and 213 nm excitation is indeed higher than that under 273 or 352 nm excitation in both Gd^{3+} and La^{3+} cases, which indicated that a quantum cutting process via cross relaxation really occurs in the samples $Ca_6Gd_{2-x}Tb_xNa_2(PO_4)_6F_2$ (x = 0.10, 0.50) with Gd^{3+} and $Ca_6La_{2-x}Tb_xNa_2(PO_4)_6F_2$ (x = 0.50, 0.90) without Gd^{3+} upon 172 and 220 nm excitation.

The above observations suggest that Gd^{3+} ions are not indispensable for QC of Tb^{3+}. However, we do not think that Gd^{3+} ions are useless for luminescence and QC of Tb^{3+}. First, at the same doping level, the whole luminescence intensity of sample $Ca_6Gd_{1.50}Tb_{0.50}Na_2(PO_4)_6F_2$ with Gd^{3+} is stronger than that of sample $Ca_6La_{1.50}Tb_{0.50}Na_2(PO_4)_6F_2$ without Gd^{3+} under the same excitation wavelengths. Second, the

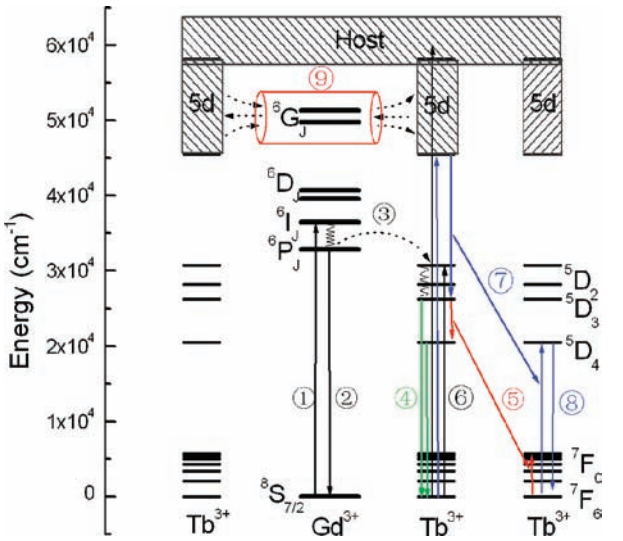

Figure 11. The schematic energy levels of Gd^{3+} and Tb^{3+} and the excitation, emission, and energy transfer processes in $Ca_6Gd_{2-x}Tb_xNa_2(PO_4)_6F_2$.

$^5D_4/^5D_3$ emission intensity ratio of sample $Ca_6Gd_{1.50}Tb_{0.50}Na_2(PO_4)_6F_2$ is larger than that of sample $Ca_6La_{1.50}Tb_{0.50}Na_2(PO_4)_6F_2$ under the same excitation wavelengths, as shown in Figure 12 and Table 1. In addition, it can be found that the $^5D_4/^5D_3$ emission intensity ratio of the Gd^{3+}-containing sample $Ca_6Gd_{1.90}Tb_{0.10}Na_2(PO_4)_6F_2$ and La^{3+}-containing sample $Ca_6La_{1.50}Tb_{0.50}Na_2(PO_4)_6F_2$ is nearly equivalent, and a similar phenomenon occurs in the samples $Ca_6Gd_{1.50}Tb_{0.50}Na_2(PO_4)_6F_2$ and $Ca_6La_{1.10}Tb_{0.90}Na_2(PO_4)_6F_2$. For Gd^{3+}-containing samples, the QC can be clearly observed when the doping content is above an x value of 0.10, but for La^{3+}-containing samples the QC cannot be clearly observed before doping level x = 0.50. At a relatively lower Tb^{3+} doping concentration, the QC can be realized in Gd^{3+}-containing samples. These phenomena indicate that Gd^{3+} ions are crucial for high QC efficiency and high quantum yield at an exact Tb^{3+} doping level. We think the higher excited 4f multiplets of Gd^{3+} around the VUV range and the intermediate role of Gd^{3+} in the energy transfer process are essential for these effects. As demonstrated in Figure 11 (process 9), the highly energetic ^6G_J multiplets of Gd^{3+} provide a route or a bridge which is favorable for energy flux between the 5d states of adjacent Tb^{3+} ions, and this phenomenon cannot occur in the La^{3+} cases. Energy flux makes the occurrence of cross relaxation (process 7) between neighboring Tb^{3+} ions quicker and more frequent. Hence, a high QC efficiency can be obtained at lower concentrations for Gd-containing samples than for La-containing samples. In addition, the well-known energy transfer by $^6I_J/^6P_J$ states through the Gd^{3+} sublattice also reinforces the luminescence efficiency.[20−22]

The cross relaxation efficiency (η) is estimate roughly by eq 3 as follows in these systems.

$$\eta = \frac{P_{(QC)^5D_4} - P_{(NQC)^5D_4}}{P_{(NQC)^5D_4}} \quad (3)$$

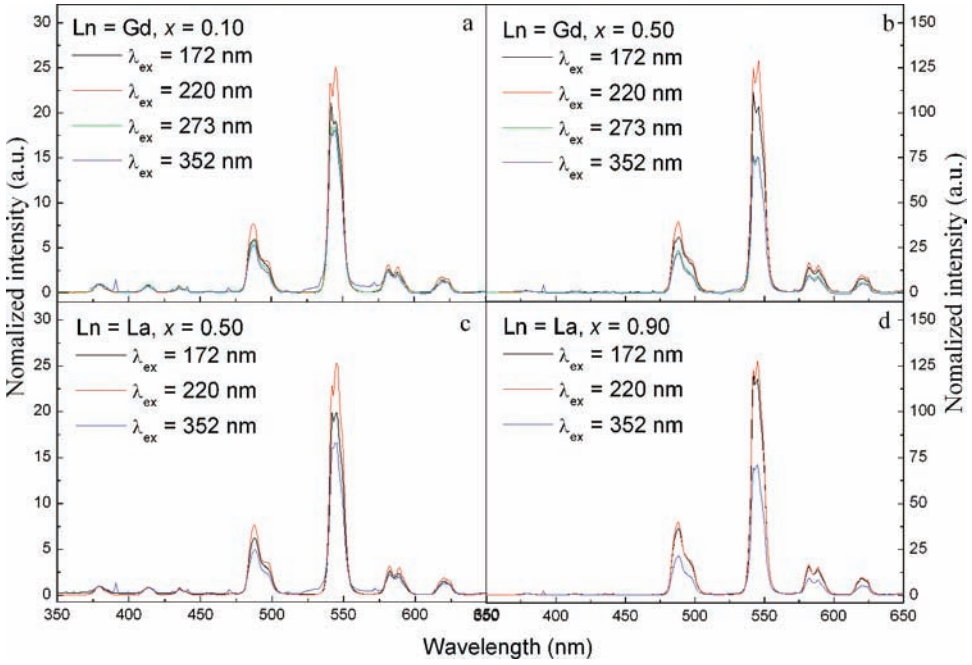

Figure 12. Emission spectra of samples $Ca_6Gd_{2-x}Tb_xNa_2(PO_4)_6F_2$ (x = 0.10, 0.50) under 172, 220, 273, and 352 nm excitation and that of samples $Ca_6La_{2-x}Tb_xNa_2(PO_4)_6F_2$ (x = 0.50, 0.90) under 172, 220, and 352 nm excitation (the spectra have been normalized to the height of Tb^{3+} $^5D_3-^7F_6$ emission at 379 nm).

Table 1. Relative Height of $^5D_4 \rightarrow {}^7F_5$ Transition (H) and Cross Relaxation Efficiencies (η) of Samples $Ca_6Gd_{2-x}Tb_xNa_2(PO_4)_6F_2$ ($x = 0.10, 0.50$) and $Ca_6La_{2-x}Tb_xNa_2(PO_4)_6F_2$ ($x = 0.50, 0.90$) under Different Excitations (Spectra Have Been Normalized to the Height of Tb^{3+} $^5D_3 - {}^7F_6$ Emission at 379 nm)

	$Ca_6Gd_{1.9}Tb_{0.1}Na_2(PO_4)_6F_2$		$Ca_6La_{1.5}Tb_{0.5}Na_2(PO_4)_6F_2$		$Ca_6Gd_{1.5}Tb_{0.5}Na_2(PO_4)_6F_2$		$Ca_6La_{1.1}Tb_{0.9}Na_2(PO_4)_6F_2$	
excitation wavelength (nm)	H	η	H	η	H	η	H	η
172	~21	~17%	~20	~18%	~111	~46%	~121	~70%
220	~25	~39%	~25	~47%	~129	~70%	~128	~80%
273	~19				~77			
352	~18		~17		~76		~71	
Figure	7a		7c		7b		7d	

Here, $P_{(QC)^5}D_4$ is the percentage of $^5D_4$ emission in the whole Tb^{3+} emission when the QC process occurs, while $P_{(QC)^5}D_4$ is the percentage of $^5D_4$ emission when the QC process does not occur. As an estimate, we ignored possible nonradiative losses such as energy migration at defects and impurities in samples, VUV absorption of phosphors, and supposed the direct energy transfer efficiency between Tb^{3+} ions or in the Tb^{3+} ion itself was 100%. The cross relaxation efficiency (η) was calculated as listed in Table 1. The lower value for excitation at 172 nm than that for excitation at 220 nm in the same sample indicates a significant fraction of excitation energy being lost nonradiatively during the quantum cutting process.

5. Conclusions

Series of phosphors $Ca_6Ln_{2-x}Tb_xNa_2(PO_4)_6F_2$ (Ln = La, Gd) were prepared using a high-temperature solid-state reaction technique. It is found that the phosphors $Ca_6Gd_{2-x}Tb_xNa_2(PO_4)_6F_2$ show strong absorption in the VUV range and have intense emission upon 172 nm excitation, but VUV range absorption is relatively weaker in the phosphors $Ca_6La_{2-x}Tb_xNa_2(PO_4)_6F_2$. The emission color of both two phosphors can be tuned from blue to yellow-green by changing the doping concentration of Tb^{3+} ions due to $^5D_3 - {}^5D_4$ cross relaxation. Visible quantum cutting through cross-relaxation Tb^{3+} (^7D_J) + Tb^{3+} ($^7F_6$) $\rightarrow$ Tb^{3+} ($^5D_3$) + Tb^{3+} ($^5D_4$) occurs in the high Tb^{3+} content samples $Ca_6Gd_{2-x}Tb_xNa_2(PO_4)_6F_2$ ($x = 0.10, 0.50$) and $Ca_6La_{2-x}Tb_xNa_2(PO_4)_6F_2$ ($x = 0.50, 0.90$) under 172 and 220 nm excitation. By comparing the VUV−vis spectroscopic properties of these phosphors, it has been found that the Gd^{3+} ions play an important intermediate role in energy transfer to convert VUV light to visible light and reinforce the cross relaxation efficiency during the quantum cutting process. Furthermore, efficient energy transfer from Gd^{3+} to Tb^{3+} was observed in a photoluminescence spectra and decay curves investigation in phosphors $Ca_6Gd_{2-x}Tb_xNa_2(PO_4)_6F_2$.

Acknowledgment. The work is financially supported by the National Basic Research Program of China (973 Program; Grant No. 2007CB935502), the National Natural Science Foundation of China (Grant Nos. 20871121 and 10979027), and the Natural Science Foundation of Guangdong Province (Grant No. 9151027501000003).